



Doping effects on complex perovskite $\text{Ba}_3\text{Ca}_{1.18}\text{Nb}_{1.82}\text{O}_{9-\delta}$ intermediate temperature proton conductor

Siwei Wang^a, Fei Zhao^a, Lingling Zhang^a, Kyle Brinkman^b, Fanglin Chen^{a,*}

^a Department of Mechanical Engineering, University of South Carolina, Columbia, SC 29208, USA

^b Materials Science & Technology Directorate, Savannah River National Laboratory, Aiken, SC 29808, USA

ARTICLE INFO

Article history:

Received 31 March 2011
Received in revised form 30 April 2011
Accepted 6 May 2011
Available online 17 May 2011

Keywords:

Proton conductor
Complex perovskite
XPS analysis
Stability
Thermal expansion coefficient

ABSTRACT

In this work, the effects of Ce doping on the Ca and Nb ions in complex perovskite $\text{Ba}_3\text{Ca}_{1.18}\text{Nb}_{1.82}\text{O}_{9-\delta}$ (BCN18) proton conductor have been evaluated. It has been found that cerium ions can be doped into both the Ca and Nb sites to form a single-phase complex perovskite structure when the sintering temperature is 1550 °C. Ce ions substituted with Nb ions enhances the electrical conductivity, especially the grain boundary conductivity. The highest conductivity has been obtained for a composition of $\text{Ba}_3\text{Ca}_{1.18}\text{Nb}_{1.62}\text{Ce}_{0.2}\text{O}_{9-\delta}$, possessing a conductivity of $2.69 \times 10^{-3} \text{ S cm}^{-1}$ at 550 °C in wet H_2 , a 78% enhancement compared with BCN18 ($1.51 \times 10^{-3} \text{ S cm}^{-1}$). The chemical stability tests show that Ce-doped BCN18 samples remain single phase after treated either in boiling water for 7 h or in pure CO_2 for 4 h at 700 °C. This work has demonstrated a new direction in developing intermediate temperature proton conducting materials that possess both high conductivity and good stability.

© 2011 Elsevier B.V. All rights reserved.

1. Introduction

Intermediate temperature proton conductors such as BaCeO_3 , BaZrO_3 , SrCeO_3 and SrZrO_3 have been extensively studied in the past three decades due to their low activation energy and high proton conductivity [1–3]. These intermediate temperature proton conductors can be used in a wide variety of applications such as proton conducting solid oxide fuel cells, intermediate temperature hydrogen sensors, hydrogen separation membranes and hydrogen pumps [4,5]. The proton conduction originates from the protonic defects in the ABO_3 perovskites due to dissociative adsorption of water or hydrogen [6]:



where $\text{OH}_\text{O}^\bullet$ represents proton charge carrier formed within the structure by attaching to the lattice oxygen. In order to achieve appreciable proton conductivity, trivalent ions are typically doped into B-sites to create oxygen vacancies. Among them, doped barium cerates, $\text{BaCe}_{1-x}\text{A}_x\text{O}_{3-\delta}$ ($\text{A} = \text{Ln}^{3+}$, $\delta = x/2$) have exhibited particularly high conductivity (within the order of $10^{-2} \text{ S cm}^{-1}$ at 600 °C) [7–12]. However, barium cerates can easily decompose into cerium

oxide and barium carbonate at elevated temperatures in CO_2 even at low CO_2 levels, or into cerium oxide and barium hydroxide in humid atmospheres [9,13–15]. Chemical instability thus raises concerns of the applications based on these materials, such as performance degradation in fuel cell tests [16]. One approach to solve this problem is to prepare mixed barium cerate/barium zirconate solid solution. Although zirconate-based proton conductors are relatively more stable at elevated temperatures in CO_2 or in humid atmospheres, they have much lower conductivity [17–20]. Consequently, an enhancement of the chemical stability can be achieved in such solid solutions with relatively high Zr content, but with substantial sacrifice of the proton conductivity [17,21,22].

In addition to simple perovskite proton conductors, there are complex perovskites which may also show proton conduction given the appropriate degree of oxygen nonstoichiometry. In the complex perovskites, the B sites are usually occupied by ions from two or more different elements and can be categorized by the differences in the valences of the B site cations. The first category of these complex perovskites is a double perovskite with $\text{A}_2(\text{B}'\text{B}'')\text{O}_6$ perovskite structure. In this case the B' and B'' ions have valences 3+ and 5+, respectively [23]. In the second category, B' and B'' ions are 2+ and 5+, respectively, forming $\text{A}_3(\text{B}'\text{B}'')_2\text{O}_9$ triple perovskite [24–26]. Among the complex perovskites, $\text{Ba}_3\text{Ca}_{1.18}\text{Nb}_{1.82}\text{O}_{9-\delta}$ (BCN18), in which Ca^{2+} and Nb^{5+} ions are taken off stoichiometry by 18% (in opposite directions) to create negatively charged defects with which oxygen vacancies and/or protons can compensate, has been demonstrated almost pure proton conduction in reducing atmospheres [23,27–29]. Further, BCN18 has shown remarkable

* Corresponding author. Tel.: +1 803 777 4875; fax: +1 803 777 0106.
E-mail address: chenfa@cec.sc.edu (F. Chen).

chemical stability in CO₂ and water vapor environment at elevated temperatures [30,31]. However, these impressive characteristics have not attracted too much attention because the relatively low conductivity hinders its practical applications where high proton conductivity is typically required.

Hence the objective of the current work is to improve the conductivity of BCN18 while retaining its chemical stability. As it is known that the choice of 1.18 for Ca sites is based on the ordering structure of B-sites ions: when the ratio of Ca²⁺ reaches 1.18, the B-sites ions are more randomly distributed, which is more favored on conductivity compared with pure Ba₃CaNb₂O₉ [27]. In this study we are exploring B sites doping for BCN18 with Ce⁴⁺ (0.87 Å), which has smaller ionic radius than Ca²⁺ (1.00 Å) but larger ionic radius than Nb⁵⁺ (0.64 Å), in order to further decrease the B sites ordering status as well as change the concentration of the oxygen vacancies for a more favored electrical conductivity. The B sites nonstoichiometry of Ba₃Ca_{1.18}Nb_{1.82}O_{9-δ} (BCN18) is maintained at Ca 18% off, by doping different amount of Ce ions into either the B' or B'' sites of BCN18, namely Ba₃Ca_{1.08}Ce_{0.1}Nb_{1.82}O_{9-δ} (B(CC0.1)N), Ba₃Ca_{1.18}Nb_{1.72}Ce_{0.1}O_{9-δ} BC(NC0.1), and Ba₃Ca_{1.18}Nb_{1.62}Ce_{0.2}O_{9-δ} BC(NC0.2), aiming at enhancing the disordering status while changing the concentration of the oxygen vacancies in the material. The phase structures and electrical properties of the doping effects are investigated. The chemical stability such as resistance to water and CO₂ of the materials are also evaluated. As very few studies of the substitution on the B-sites in BCN18 have been reported before, this preliminary work is expected to stimulate further studies, especially by exploring other potential B-site dopants of BCN18 in the pursuit of novel proton conducting materials.

2. Experimental

The Ce-doped BCN18 samples were prepared by a conventional solid state reaction method [13,20,32]. Stoichiometric amount of BaCO₃ (Alfa Aesar, 99.8%), CaCO₃ (Alfa Aesar, 99.5%), Nb₂O₅ (Alfa Aesar, 99.9%) and CeO₂ (Alfa Aesar, 99.9%) were mixed together by ball-milling in ethanol for 24 h. After drying, the obtained powders were pressed into pellets, followed by calcining at 1200 °C for 5 h in air with a heating rate of 3 °C min⁻¹. The pellets were then grinded into powders which were subsequently mixed with 5 wt% polyvinyl alcohol (PVA) binder and uniaxially pressed into pellets under a pressure of 400 MPa. The green pellets were sintered at 1550 °C for 5 h in air with a heating rate of 2 °C min⁻¹.

X-ray diffractometer (Rigaku, Japan) with graphite-monochromatized Cu Kα radiation (λ1.5418 Å) was employed to record the X-ray diffraction patterns (XRD) of the samples. Scanning electron microscopy (SEM, FEI Quanta and XL 30) was used to characterize the morphology and micro-structures of the sintered pellets. For electrical conductivity measurements, the sintered pellets were polished and applied with platinum paste on both sides and then baked at 950 °C for 30 min to form the current collector. Platinum wires were attached to the surfaces of the Pt current collector. Electrical conductivity tests were conducted using AC impedance spectra with built-in impedance analyzer (Versa STAT3-400, Princeton Applied Research) in the frequency range from 0.1 Hz to 1 MHz at different testing environments. The wet atmospheres used in this study contain 3 vol% H₂O, obtained by flowing gas through a water bubbler at room temperature. The sintered pellets were also exposed to either boiling water or CO₂ atmosphere at high temperatures. After exposure, XRD patterns of the surfaces of the pellets were characterized. Thermal expansion coefficient measurement of the sintered sample was measured using a NETZSCH DIL 402C pushrod dilatometer from room temperature to 1000 °C with a heating rate of 5 °C min⁻¹.

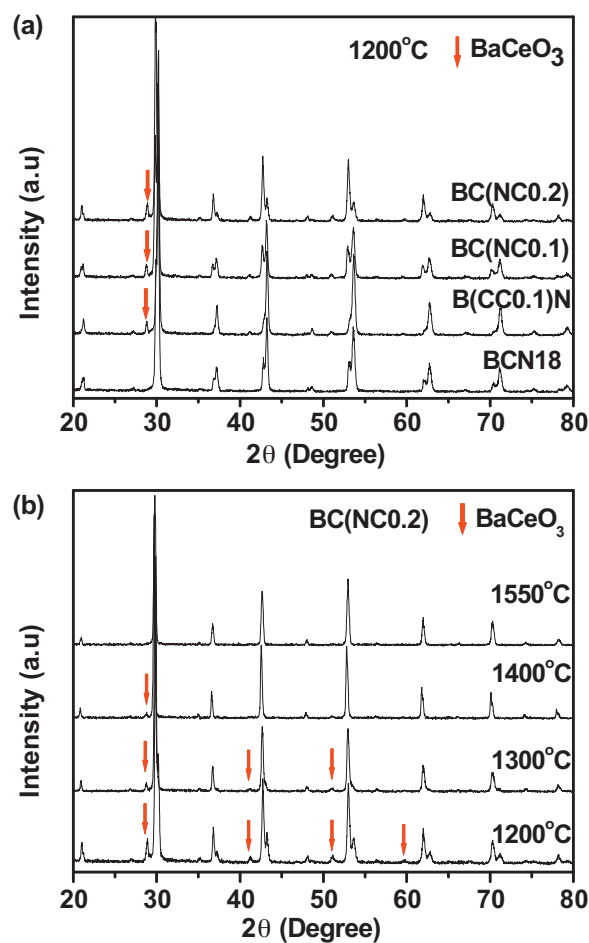


Fig. 1. (a) XRD patterns of samples calcined at 1200 °C for 5 h; (b) XRD patterns of BC(NC0.2) calcined at different temperatures. The arrows correspond to the BaCeO₃ impurity peaks.

3. Results and discussion

3.1. XRD analysis

Fig. 1(a) shows the XRD patterns of different samples prepared at 1200 °C for 4 h. The calcined powders are composed primarily of the cubic perovskite phase, with BaCeO₃ impurity phase present upon doping of Ce ions in the B sites, as noted in Fig. 1(a) with arrows. The majority perovskite structure may thus be Ba deficient due to the formation of BaCeO₃ secondary phase. As the calcination temperature increases, Ce ions gradually dissolve into the complex perovskite structure. As an example, XRD patterns of BC(NC0.2) calcined at different temperatures are shown in Fig. 1(b). The result indicates that the solubility of dopants can be tuned to a higher extent by increasing the calcination temperature, similar to that of BaCeO₃ based proton conductors [33]. The peak split of the XRD patterns indicative of two phase structures may be caused by the coexistence of unhydrated and hydrated phases of the powders. As the calcination temperature is further increased, the unhydrated phase will be dominant. Similar phenomena on Ba₃Ca_{1.18}Ta_{1.82}O_{8.73}, Ba_{0.5}In_{0.5}ZrO_{3-δ} and Sr₃Ca_{1+x}Nb_{2-x}O_{9-δ} systems have also been reported [34,35].

Fig. 2 shows the XRD patterns of the samples sintered at 1550 °C for 5 h. Single cubic complex perovskite structure with no secondary phases is obtained for all the samples, showing that BaCeO₃ has reacted with the nonstoichiometric perovskite phase completely. Weak (1 1 1) peaks at 2θ angle around 18.2° are an

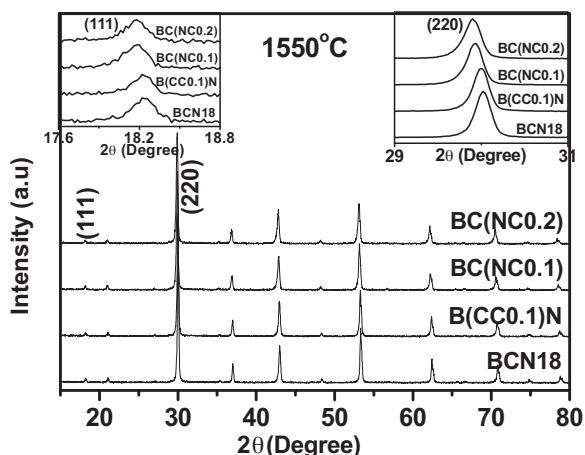


Fig. 2. XRD patterns of samples sintered at 1550 °C for 5 h, with step scan of (1 1 1) and (2 2 0) peaks in the inset pictures.

indication of B site 1:1 ordering of the perovskite structure for all the samples (shown in Fig. 2 inset for the (1 1 1) step scan). The lattice parameters for the samples are 8.4095, 8.4149, 8.433 and 8.442 Å for BCN18, B(CC0.1)N, BC(NC0.1) and BC(NC0.2), respectively, consistent with step scan results of (2 2 0) peaks which shows a peak shift to a lower 2θ degree (shown in Fig. 2 inset). For pure BCN18, it is B site 1:1 ordering mixed with random ordering [27]. The introduction of Ce^{4+} (0.87 Å) into either Ca^{2+} (1.00 Å) sites or Nb^{5+} (0.64 Å) sites would promote the B-sites-disordering of the structure, which would be expected to increase the ion mobility and consequently enhance the ionic conductivity [36]. However, for sample B(CC0.1)N, a decrease in lattice parameter, with expectation of Ce^{4+} (0.87 Å) substitution on Ca^{2+} (1.00 Å), has not been observed. The increase of the lattice parameter may probably be due to the valence change of Ce^{4+} ions into Ce^{3+} ions (1.01 Å) for charge compensation consideration. Ce^{3+} is more likely to substitute into Ca^{2+} site because its ionic radius is more closely matched to that of Ca^{2+} . This will in turn deteriorate the disordering status of BCN18 structure and results in a decreased conductivity. For BC(NC0.1) and BC(NC0.2) samples, it is consistent with the expectation that the increase in the lattice parameters is a consequence of large Ce ions (either 3+ or 4+ oxidation states) substituted into small Nb^{5+} sites and an enhancement of the conductivity has been observed.

To further determine the oxidation states of the Ce ions from the doping effect, XPS measurements were employed to obtain the Ce 3d spectra for sample B(CC0.1)N and BC(NC0.1), as shown in Fig. 3. The Ce 3d spectra for CeO_2 and $BaCe_{0.85}Y_{0.15}O_{3-\delta}$ (denoted as BCY) were also collected as references. It can be seen that for both B(CC0.1)N and BC(NC0.1) samples, the Ce-ions show a mixture of 3+ and 4+ oxidation states, indicating that Ce^{3+} and Ce^{4+} co-exist for both samples. For example, for the proposed substitution of Ce-ions into Nb^{5+} sites, there are Ce^{3+} ions that might either doped into Nb^{5+} or Ca^{2+} sites. Compared with B(CC0.1)N, the peak intensities for BC(NC0.1) are stronger at binding energy of 881 eV and 915.5 eV, which are characteristics of Ce^{4+} spectrum [37], indicating that more Ce^{4+} ions exhibited in BC(NC0.1) than that in B(CC0.1)N. Therefore, XPS results are consistent with the XRD analysis that the Ca^{2+} sites are more favorable for Ce^{3+} substitution while smaller Nb^{5+} sites are more favorable for Ce^{4+} ions substitution. It is also noted that even for $BaCe_{0.85}Y_{0.15}O_{3-\delta}$, the Ce 3d spectrum shows a mixture of 3+ and 4+ oxidation states, probably due to large covalent characteristics of the ionicity in perovskite structures [38].

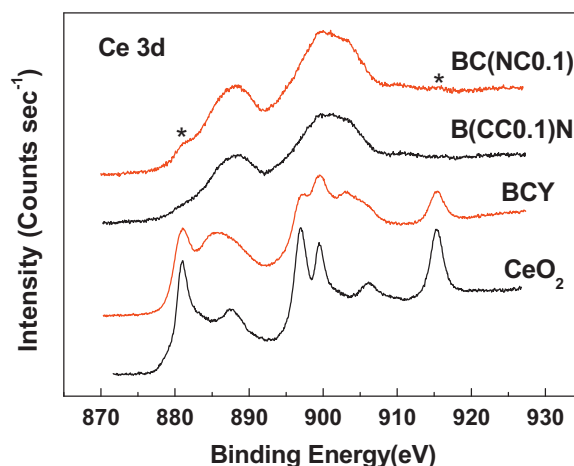


Fig. 3. XPS spectra of Ce 3d for samples BC(NC0.1), B(CC0.1)N, $BaCe_{0.85}Y_{0.15}O_{3-\delta}$ (BCY) and CeO_2 collected at room temperature.

3.2. Microstructures

The microstructures of the sintered pellets are presented in Fig. 4. The top images reveal the surface morphologies while the bottom images are the corresponding cross-sectional view of the same samples. All the samples show dense microstructures, consistent with the Archimedes density tests that all the samples have greater than 94% relative densities. The average grain sizes measured from the surface images for the sintered pellets are 3.14 ± 1.18 , 2.41 ± 0.90 , 3.57 ± 1.19 and 4.20 ± 1.60 μm , respectively, indicating that the introduction of cerium into Ca^{2+} sites will inhibit the grain growth, while the introduction of Ce ions into Nb^{5+} sites will promote the grain growth and consequently reduce the density of grain boundaries [39]. Therefore, the doping of Ce ions into either B' or B'' sites shows a clear effect on the grain growth of the sintered samples which would in turn affect the electrical performance.

3.3. Electrical conductivity

The AC impedance spectra for the samples are conducted to measure the bulk and grain boundary conductivity of the samples. Typical Nyquist plots of the impedance spectra for sample BC(NC0.2) in wet air at 122 and 200 °C are shown in Fig. 5(a) and (b), respectively. The insets are the expanded views of the high frequency regions. The impedance spectra typically have three semi-circles corresponding to the bulk, grain boundary and electrode responses from high to low frequencies. As shown in the inset of Fig. 5(a) that at 122 °C, a semicircle related to the bulk conduction process in the high frequency range (capacitance $\sim 10^{-12}$ F cm^{-1}) can be clearly seen. With the temperature increased to 220 °C, as shown in the inset of Fig. 5(b), only a portion of the semicircle corresponding to the bulk conduction response is observable in the high frequency range. When the temperature was further increased, the semicircle corresponding to the bulk conduction response can no longer be well defined and the bulk resistance can be then derived from the high frequency intercept of the intermediate frequency semicircle with the real axis. The semicircle in the intermediate frequency range is attributed to grain boundary responses (capacitance $\sim 10^{-9}$ F cm^{-1}) while the spectrum in the low frequency range is due to the electrode response (capacitance $\sim 10^{-4}$ F cm^{-1}) [22]. The other samples also have similar impedance spectrum evolution as a function of the testing temperature to that of BC(NC0.2).

Fig. 6(a) and (b) show the total conductivities of the samples in wet air and wet H_2 , respectively. It can be seen that the introduction

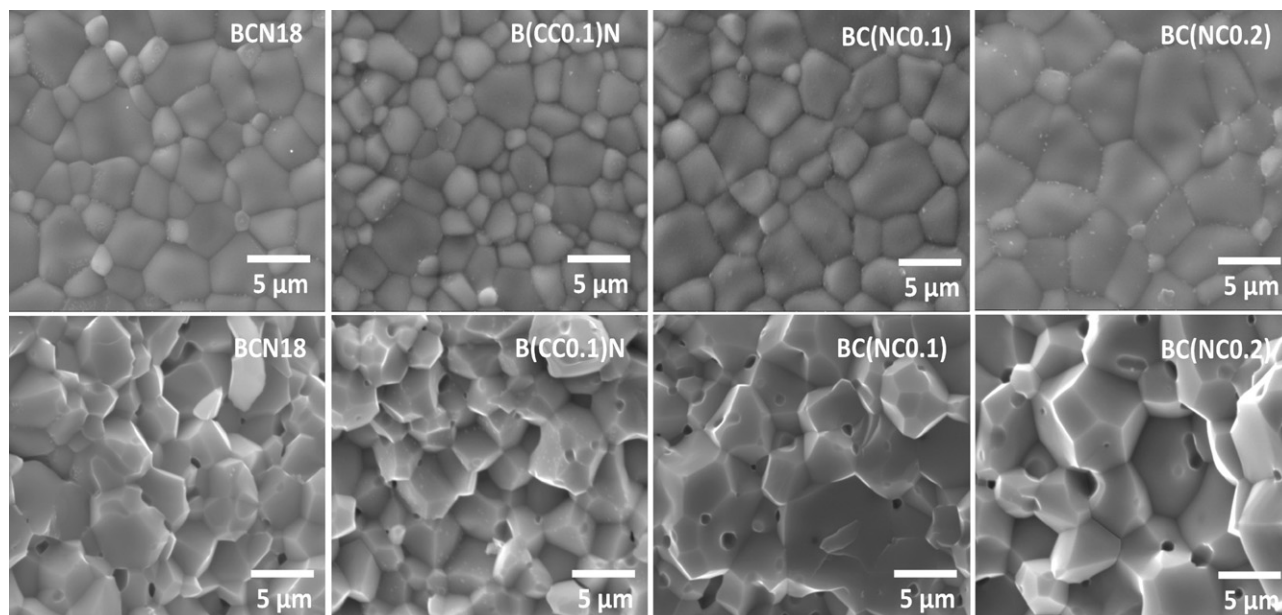


Fig. 4. SEM images of the sintered pellets. Top images: surface morphology of the pellets; bottom images: cross-section view of the pellets.

of Ce ions into either Ca or Nb sites presents a distinct effect on the conduction behavior. Sample B(CC0.1)N shows the lowest conductivity among the different samples both in air and in H₂ at the same testing conditions. As discussed above in the XRD and XPS analysis, most Ce⁴⁺ ions may probably be reduced to Ce³⁺ ions to be substituted into Ca²⁺ sites. A decrease in the grain size has also been observed for B(CC0.1)N (as shown in Fig. 4 and Table 1), resulting in an increase in grain boundary numbers and consequently an expected reduction in the total electrical conductivity. Another important factor that influences the electrical conductivity is the concentration of oxygen vacancies generated through doping. Substituting Ca²⁺ with either Ce⁴⁺ or Ce³⁺ will not lead to an increase of oxygen vacancies. Thus the decrease in conductivity for sample B(CC0.1)N can be viewed as a collective result of the above correlations. As for samples BC(NC0.1) and BC(NC0.2), the electrical conductivity are increased compared with the undoped BCN18, with sample BC(NC0.2) showing the highest conductivity among the different samples tested at similar conditions (an enhancement of 78% in electrical conductivity is achieved). Doping Ce ions (either Ce⁴⁺ or Ce³⁺) into Nb⁵⁺ sites will result in an enhancement of the B-sites disordering and an increase in the concentration of oxygen vacancies. In addition, as shown in Fig. 4, an increase in grain size has been observed for BC(NC0.1) and BC(NC0.2) compared with that of BCN18. All these factors are expected to lead to an increase in the electrical conductivity, which has been confirmed by the conductivity data in Fig. 6.

In Fig. 6(a), by linearly fitting the slopes of the Arrhenius plots, the activation energies for samples BCN18, B(CC0.1)N, BC(NC0.1) and BC(NC0.2) in wet air are calculated to be 0.77, 0.73, 0.63, and 0.47 eV, respectively, clearly showing the effect of Ce doping on the crystal structure and consequently influence on the electrical

conductivity. A larger decrease in activation energy is observed with Nb sites doped samples. This can be understood that more B-sites ions are disorderly distributed (“randomly” distributed) rather than ordered because of the Ce ions doping, thus the charged ions can move more easily, consistent with the reported data [36]. A tendency of decreased activation energy with increasing unit cell volume has also been observed for proton conductors with simple perovskite structure [40].

For samples tested in wet H₂ atmosphere as shown in Fig. 6(b), a decrease in activation energy at high temperature range (higher than 550 °C) has been observed, indicative of change in conduction mechanism. When the testing temperature increases, a decrease in proton conductivity is anticipated as a result of the dehydration of the oxide lattice due to the exothermal nature of reaction (1) [41]. A gradual change from proton conduction into mixed oxygen ion and proton conduction is expected. Electronic conduction may also exist under high temperature regime [42]. Other proton conducting materials such as BCN18, BaZr_{0.1}Ce_{0.7}Y_{0.2}O_{3-δ}, BaZr_{0.9}Y_{0.1}O_{3-δ}, and Sr₃CaZr_{0.5}Ta_{1.5}O_{8.75} also show change of shapes in the conductivity Arrhenius plots in wet H₂ atmospheres [18,23,24,43].

By separating the bulk and grain boundary conductivity, it is able to obtain detailed information on different contributions to the total conductivity. To evaluate the effect of introduction of Ce ions into Nb sites on the bulk and grain boundary conduction mechanisms, Fig. 7(a) and (b) shows the Arrhenius plots of the bulk and grain boundary conductivity for samples BCN18 and BC(NC0.1) in wet air and wet H₂, respectively. Typically it is difficult to separate the grain boundary conductivity from the bulk conductivity when the testing temperature is high, however, in our experiments, because of the unique microstructure and characteristic of the BCN18 based samples, they can be separated

Table 1
Summary of structural and electrical properties of the sintered samples.

Sample denotation	Lattice parameter (Å)	Average grain size (μm)	Conductivity @550 °C (S cm ⁻¹)	
			Wet air	Wet H ₂
BCN18 (Ba ₃ Ca _{1.18} Nb _{1.82} O _{9-δ})	8.4095	3.14	1.25 × 10 ⁻³	1.51 × 10 ⁻³
B(CC0.1) (Ba ₃ Ca _{1.08} Ce _{0.1} Nb _{1.82} O _{9-δ})	8.4149	2.41	0.719 × 10 ⁻³	0.905 × 10 ⁻³
BC(NC0.1) (Ba ₃ Ca _{1.18} Nb _{1.72} Ce _{0.1} O _{9-δ})	8.4330	3.57	1.95 × 10 ⁻³	2.13 × 10 ⁻³
BC(NC0.2) (Ba ₃ Ca _{1.18} Nb _{1.62} Ce _{0.2} O _{9-δ})	8.4420	4.01	2.42 × 10 ⁻³	2.69 × 10 ⁻³

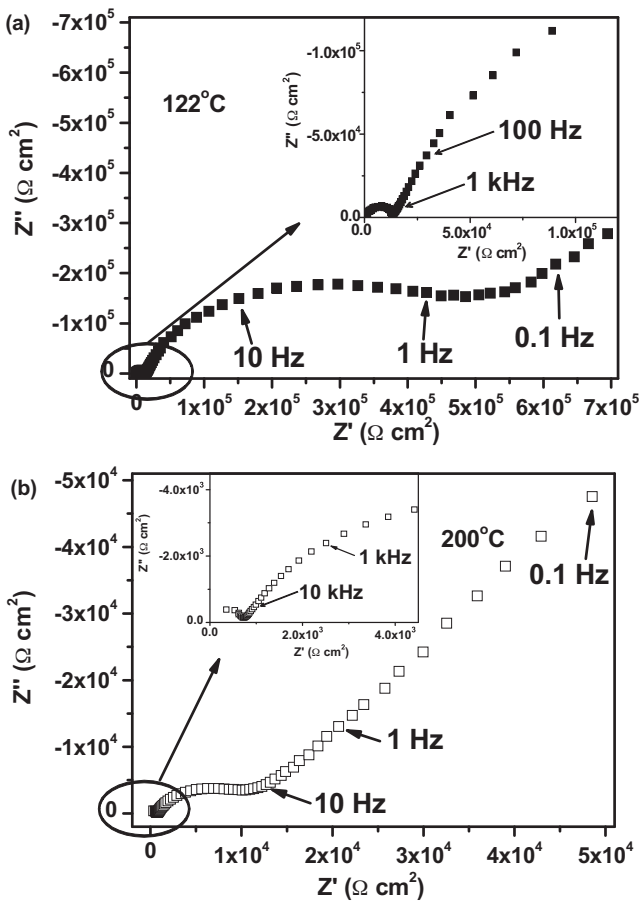


Fig. 5. Nyquist plots for BC(NC0.2) in wet air at (a) 122 °C and (b) 200 °C. Inset pictures are expanded views of high frequency regions.

up to 700 °C (see Fig. 7(a) inset). In wet air the activation energies for BCN18 bulk, BC(NC0.1) bulk, BCN18 grain boundary, and BC(NC0.1) grain boundary conduction are 0.53, 0.463, 1.10, and 1.12 eV, respectively, showing almost linear behavior in Arrhenius plots. In wet H₂ at temperatures below 550 °C, for bulk conduction, the activation energies for BCN18 and BC(NC0.1) are 0.57 and 0.55 eV, respectively. While at elevated temperatures higher than 550 °C, a decrease in activation energy for bulk conduction is clearly observed, with activation energy of 0.13 and 0.1 eV, respectively, characteristic of electronic conduction. It should be noted that the slope change of the bulk conduction proceeds gradually while there is little change for that of the grain boundary conduction. The activation energies for grain boundary conductivity are 0.88 and 0.89 eV for BCN18 and BC(NC0.1), respectively. Therefore, it can be concluded that the bowed behavior of the total conductivity plot above 550 °C is mainly attributed to the change in the mechanism of the bulk conduction.

In both air and H₂ atmospheres, substitution of Nb⁵⁺ with Ce ions leads to a decrease in activation energy as well as an increase in bulk conductivity. The activation energy for grain boundary conduction remains almost the same with different substitution of Ce ions. However, the magnitude of the grain boundary conduction is significantly enhanced because of the substitution. This can be partly reflected by the influence of the grain sizes on grain boundary conductivity, with larger grain sizes showing enhanced grain boundary conductivity. Further, perhaps more importantly, doping Ce⁴⁺ and/or Ce³⁺ ions in the Nb⁵⁺ sites may lead to an increase in oxygen vacancies in the grain boundary region, resulting in

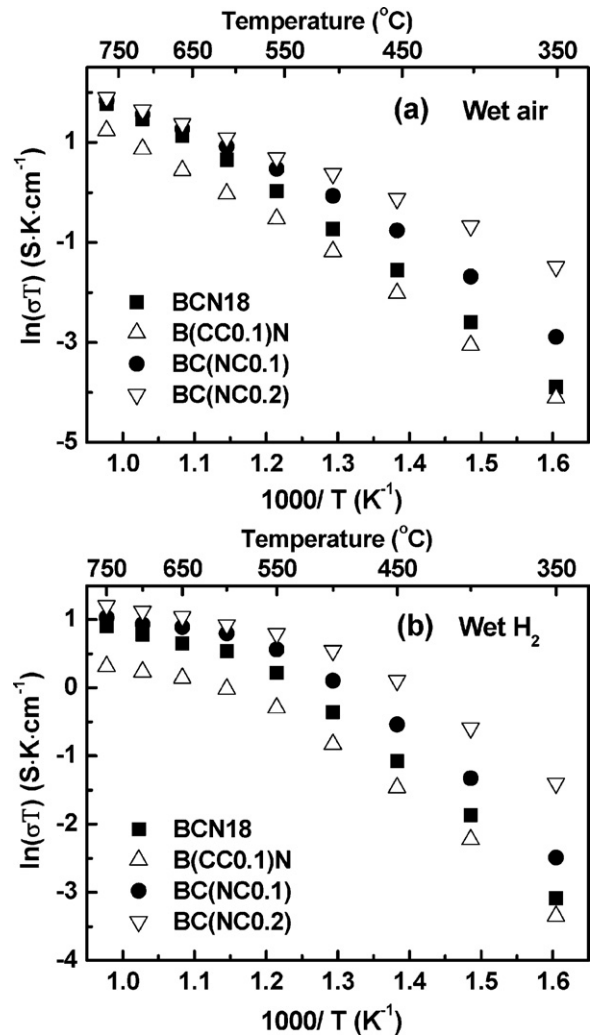


Fig. 6. Arrhenius plots of total conductivity for samples (a) in wet air and (b) in wet H₂.

higher grain boundary conductivity without changing the conduction mechanism.

It is also noticed that at temperatures lower than 550 °C, improvement of total conductivity in wet H₂ is observed compared with that in wet air for the samples, indicating enhancement of proton conduction in H₂ atmosphere (as shown in the inset in Fig. 7) [19]. Table 1 lists the conductivity values of the samples tested in different atmospheres at 550 °C.

3.4. Chemical stability

To evaluate the chemical stability of Ce doped BCN18 materials, the sintered pellets were exposed into boiling water and CO₂ atmosphere at elevated temperatures. Fig. 8(a) shows the XRD patterns of the pellets after boiling in water for 7 h. It can be seen that after boiling in water for 7 h, all the samples maintain pure perovskite structure with no detectable impurity phases. It is noticed that the peak intensity decreased after the treatment, especially for sample BC(NC0.2). This may be caused by the absorption of H₂O in the samples during treatment. FTIR spectrum study also confirmed the water adsorption on boiled Ba₃CaNb_{1.75}Ti_{0.25}O_{9-δ} samples as reported by Thangadurai and coworker [31].

The stability tests were also conducted in CO₂ atmosphere at 700 °C for 4 h as well as in wet 3 vol% CO₂ (air as the balance gas, 3 vol% H₂O) at 700 °C for 24 h, both with a flow rate of 50 mL min⁻¹

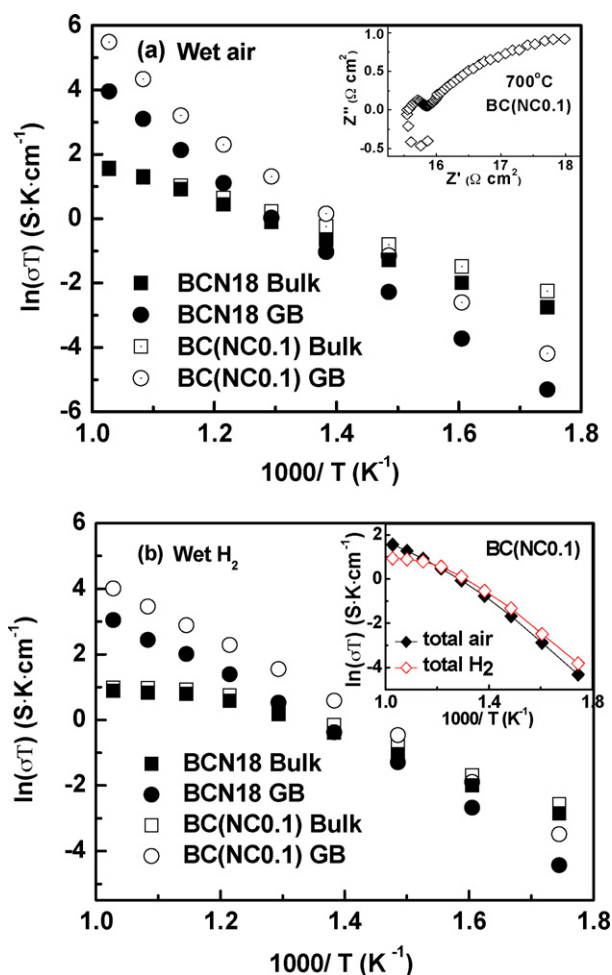


Fig. 7. Arrhenius plots of bulk and grain boundary conductivity for sample BCN18 and BC(NC0.1) in (a) wet air and (b) wet H₂. Inset (a) is the Nyquist plot for BC(NC0.1) at 700 °C in wet air and inset (b) is the Arrhenius plot for BC(NC0.1) in wet air and wet H₂.

to evaluate the stability in carbon dioxide environments. XRD patterns of the samples after exposures are presented in Fig. 8(b) and (c), respectively. It can be seen that no impurity phases have been detected for the samples treated in CO₂ environment, suggesting no reaction taken place between CO₂ and the samples. Inspection of the samples after treatments revealed no apparent change in either color or morphology of the samples, consistent with the XRD results. Consequently, the introduction of Ce ions into either B' site or B'' site did not show any detrimental effect on the chemical stability for BCN18. Combined with the conductivity results, the doped BCN18 system turns to be a very promising intermediate temperature proton conductors, with respect to the stability tests mentioned above for Ba(Ce,Zr)O₃ based simple perovskite systems. For instance, BaCe_{0.7}Zr_{0.2}Y_{0.1}O_{3-δ} will decompose when either treated in boiling water for 6 h or held in carbon dioxide atmosphere for 2 h at 900 °C [17]; even for BaCe_{0.3}Zr_{0.5}Y_{0.2}O_{3-δ}, impurity phase is formed after exposure to CO₂ at 900 °C for 3 h [21]. BaCe_{0.45}Zr_{0.45}Sc_{0.2}O_{3-δ} has been reported to be stable in pure CO₂ up to 900 °C, but the total conductivity is relatively low, only 4.49×10^{-4} S cm⁻¹ at 600 °C in air [22].

3.5. Thermal expansion coefficient

The thermal expansion coefficient (TEC) matching among the components in a device is of crucial importance for real applications in order to minimize the thermally induced stresses during

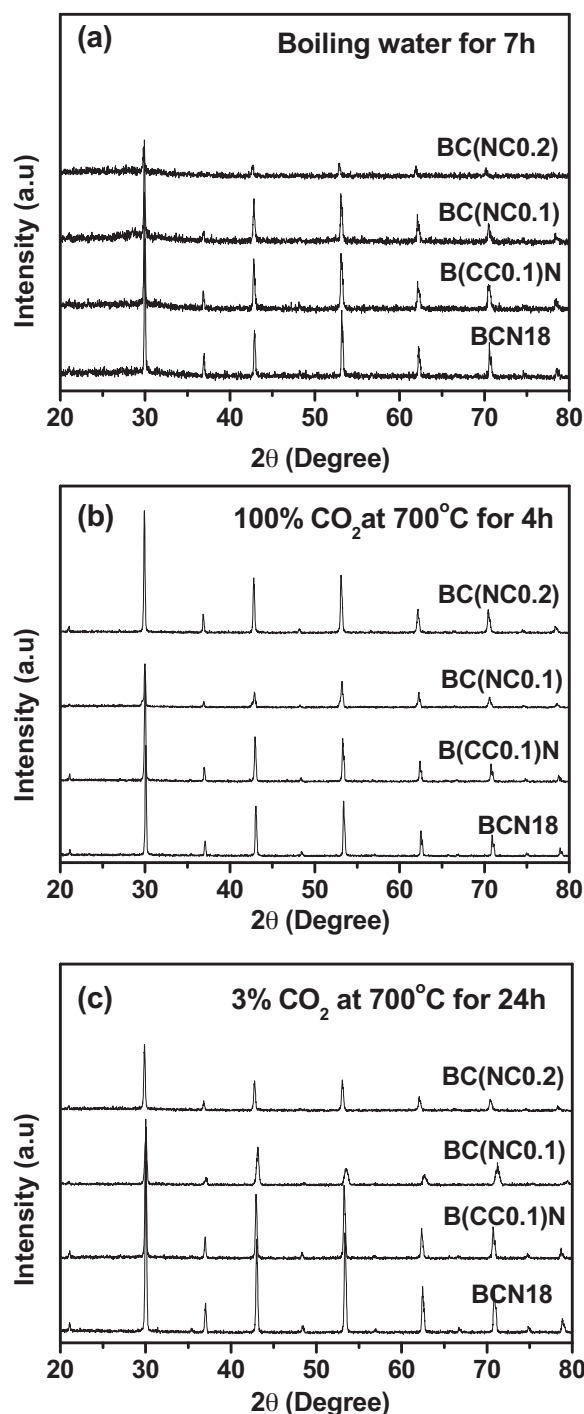


Fig. 8. (a) XRD patterns of the sintered pellets after exposure in boiling water for 7 h; (b) XRD patterns of the sintered pellets after exposure in 100% CO₂ at 700 °C for 4 h; (c) XRD patterns of the sintered pellets after exposure in 3% CO₂ + 3% H₂O at 700 °C for 24 h.

the thermal cycling process. For instance, TEC mismatch between the electrolyte and the cathode in SOFCs can potentially lead to cracking in the electrolyte–cathode interface, and even to the spallation of the cathode from the electrolyte surface. Fig. 9 shows the thermal expansion behavior of sample BC(NC0.2) measured in air and 5% H₂/95% N₂ forming gas from 150 to 1000 °C. Almost linear curves are obtained in the entire temperature range studied, indicating no structural transformation within this temperature range. The TEC value from 150 to 1000 °C for BC(NC0.2) is calculated to be 14.73×10^{-6} and 15.03×10^{-6} K⁻¹ in air and in

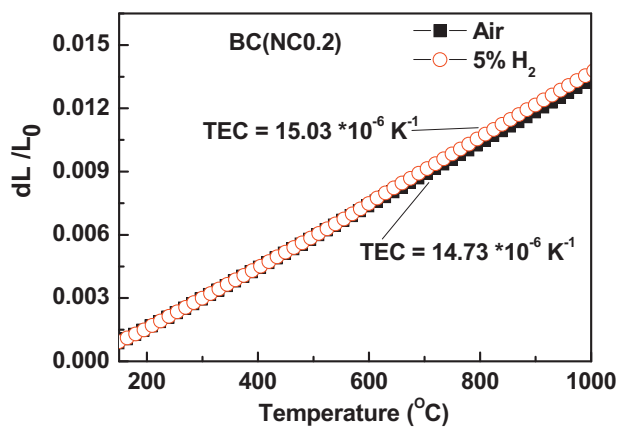


Fig. 9. Thermal expansion behavior of BC(NC0.2) sintered pellets in air and in forming gas with 5% H₂ balanced with 95% N₂.

5% H₂, respectively. The lattice expansion observed at elevated temperatures in reducing atmosphere may be attributed to the loss of lattice oxygen and the formation of oxygen vacancies due to low oxygen partial pressure [44]. The TEC values show good compatibility with typical intermediate temperature cathode materials such as La_{0.6}Sr_{0.4}Co_{0.2}Fe_{0.8}O_{3- δ} ($17.5 \times 10^{-6} \text{ K}^{-1}$) and BaCo_{0.7}Fe_{0.2}Nb_{0.1}O_{3- δ} ($14.64 \times 10^{-6} \text{ K}^{-1}$ from 200 to 1000 °C) [45,46], indicating that doped BCN18 can be potentially applied as the electrolytes for intermediate-temperature SOFCs.

4. Conclusions

The effects on Ce ions substituted with either Ca or Nb for Ba₃Ca_{1.18}Nb_{1.82}O_{9- δ} have been investigated. The following conclusions have been obtained:

- (1) By sintering at 1550 °C for 5 h, single phase complex perovskite structure has been formed for all the samples studied. Ce ions showed mixed oxidation states for both substitutions, with more 4+ oxidation states for Nb substitution. Ce substituted with Nb ions promoted the grain growth and enhanced electrical conductivity, especially the grain boundary conductivity.
- (2) The introduction of Ce ions into Ca and/or Nb sites does not show any detrimental effect on the chemical stability for BCN18 system, demonstrating very satisfactory chemical stability compared with that of cerate based simple perovskite proton conductor systems.
- (3) The thermal expansion coefficient value is larger than conventional electrolyte materials, showing good compatibility with typical intermediate temperature cathode materials in SOFC area.

Overall, an optimum composition of Ba₃Ca_{1.18}Nb_{1.62}Ce_{0.2}O_{9- δ} has been achieved, possessing both high proton conductivity and good stability in the intermediate temperature range.

Acknowledgements

The authors acknowledge gratefully the financial support of the Department of Energy Nuclear Energy University Program (NEUP) (award no. 10-681).

References

- [1] H. Iwahara, T. Esaka, H. Uchida, N. Maeda, *Solid State Ionics* 3–4 (1981) 359.
- [2] K.D. Kreuer, *Annu. Rev. Mater. Res.* 33 (2003) 333.
- [3] B.C.H. Steele, A. Heinzl, *Nature* 414 (2001) 345.
- [4] K.D. Kreuer, S. Adams, W. Münch, A. Fuchs, U. Klock, J. Maier, *Solid State Ionics* 145 (2001) 295.
- [5] F. Zhao, Q. Liu, S. Wang, K. Brinkman, F. Chen, *Int. J. Hydrogen Energy* 35 (2010) 4258.
- [6] I. Kosacki, H.L. Tuller, *Solid State Ionics* 80 (1995) 223.
- [7] F. Chen, P. Wang, O.T. Sorensen, G. Meng, D. Peng, *J. Mater. Chem.* 7 (1997) 1533.
- [8] R. Peng, Y. Wu, L. Yang, Z. Mao, *Solid State Ionics* 177 (2006) 389.
- [9] Z. Wu, M. Liu, *J. Electrochem. Soc.* 144 (1997) 2170.
- [10] S. Yamaguchi, N. Yamada, *Solid State Ionics* 162–163 (2003) 23.
- [11] K. Künnstler, H.J. Lang, A. Maiwald, G. Tomandl, *Solid State Ionics* 107 (1998) 221.
- [12] M. Amsif, D. Marrero-Lopez, J.C. Ruiz-Morales, S.N. Savvin, M. Gabbás, P. Nunez, *J. Power Sources* 196 (2011) 3461.
- [13] F. Chen, O.T. Sorensen, G. Meng, D. Peng, *J. Mater. Chem.* 7 (1997) 481.
- [14] S. Wang, F. Zhao, L. Zhang, K. Brinkman, F. Chen, *J. Alloys Compd.* 506 (2010) 263.
- [15] Z. Tao, Z. Zhu, H. Wang, W. Liu, *J. Power Sources* 195 (2010) 3481.
- [16] F. Zhao, F. Chen, *Int. J. Hydrogen Energy* 35 (2010) 11194.
- [17] Z. Zhong, *Solid State Ionics* 178 (2007) 213.
- [18] C. Zuo, S. Zha, M. Liu, M. Hatano, M. Uchiyama, *Adv. Mater.* 18 (2006) 3318.
- [19] S. Barison, M. Battagliarin, T. Cavallin, L. Doubova, M. Fabrizio, C. Mortalo, S. Boldrini, L. Malavasi, R. Gerbasi, *J. Mater. Chem.* 18 (2008) 5120.
- [20] L. Yang, S. Wang, K. Blinn, M. Liu, Z. Liu, Z. Cheng, M. Liu, *Science* 326 (2009) 126.
- [21] E. Fabbri, A. D'Epifanio, E. Di Bartolomeo, S. Licoccia, E. Traversa, *Solid State Ionics* 179 (2008) 558.
- [22] A.K. Azad, J.T.S. Irvine, *Solid State Ionics* 178 (2007) 635.
- [23] H.G. Bohn, T. Schober, T. Mono, W. Schilling, *Solid State Ionics* 117 (1999) 219.
- [24] D.J.D. Corcoran, J.T.S. Irvine, *Solid State Ionics* 145 (2001) 307.
- [25] H.D.A.L. Viana, J.T.S. Irvine, *Solid State Ionics* 178 (2007) 717.
- [26] K. Oikawa, T. Kamiyama, S. Ikeda, T. Shishido, S. Yamaguchi, *Solid State Ionics* 154–155 (2002) 641.
- [27] A.S. Nowick, Y. Du, *Solid State Ionics* 77 (1995) 137.
- [28] S. Valkenberg, H.G. Bohn, W. Schilling, *Solid State Ionics* 97 (1997) 511.
- [29] H.d.A.L. Viana, J.T.S. Irvine, *J. Mater. Chem.* 20 (2010) 8506.
- [30] D. Hassan, S. Janes, R. Clasen, *J. Eur. Ceram. Soc.* 23 (2003) 221.
- [31] T.T. Trinh, V. Thangadurai, *Electrochim. Acta* 56 (2010) 227.
- [32] S. Wang, J. Zhai, X. Chou, L. Zhang, X. Yao, *Mater. Chem. Phys.* 115 (2009) 200.
- [33] N. Bonanos, K.S. Knight, B. Ellis, *Solid State Ionics* 79 (1995) 161.
- [34] J.T.S. Irvine, D.J.D. Corcoran, J. Canales-Vazquez, *Solid State Ionics* 152–153 (2002) 749.
- [35] J.T.S. Irvine, M.C. Verbraeken, H. Viana, A.K. Azad, I. Ahmed, S. Eriksson, The 15th International Conference on Solid State Protonic Conductors Oral 09, 2010.
- [36] A.S. Nowick, Y. Du, K.C. Liang, *Solid State Ionics* 125 (1999) 303.
- [37] J.-T. Shiu, T.-T. Fang, *J. Am. Ceram. Soc.* 87 (2004) 391.
- [38] T. Schober, K. Szot, M. Barton, B. Kessler, U. Breuer, H.J. Penkalla, W. Speier, *J. Solid State Chem.* 149 (2000) 262.
- [39] Y. Yamazaki, R. Hernandez-Sanchez, S.M. Haile, *Chem. Mater.* 21 (2009) 2755.
- [40] K.H. Ryu, S.M. Haile, *Solid State Ionics* 125 (1999) 355.
- [41] H. Fjeld, D.M. Kepaptsoglou, R. Haugsrud, T. Norby, *Solid State Ionics* 181 (2009) 104.
- [42] K. Katahira, Y. Kohchi, T. Shimura, H. Iwahara, *Solid State Ionics* 138 (2000) 91.
- [43] G.B. Hans, S. Tilman, *J. Am. Ceram. Soc.* 83 (2000) 768.
- [44] V. Prashanth Kumar, Y.S. Reddy, P. Kistaiah, G. Prasad, C. Vishnuvardhan Reddy, *Mater. Chem. Phys.* 112 (2008) 711.
- [45] H. Ullmann, N. Trofimenko, F. Tietz, D. Stöver, A. Ahmad-Khanlou, *Solid State Ionics* 138 (2000) 79.
- [46] Z. Liu, L. Cheng, M. Han, *J. Power Sources* 196 (2011) 868.